

Segmentation and Morphology of the Central Indian Ridge between 3°S and 11°S, Indian Ocean

K. A. Kamesh Raju¹, Kiranmai Samudrala¹, R. K. Drolia², Dileep Amarnath³, Ratheesh Ramachandran⁴, Abhay Mudholkar¹

¹National Institute of Oceanography, Dona Paula, Goa – 403004, India

²Retired Scientist, National Geophysical Research Institute, Hyderabad-500007, India

³Upstream Petroleum Consultants, P.B. No. 72678, Dubai, UAE

⁴National Center for Antarctic and Ocean Research, Vasco-Da-Gama, Goa, India

Abstract

The segmentation pattern of 750 km long Central Indian Ridge (CIR) between 3°S and 11°S latitudes in the Indian Ocean has been studied using multibeam bathymetry and magnetic data. Twelve ridge segments were identified that are separated by well defined transform faults and non-transform discontinuities. Magnetic model studies qualify the ridge as a slow spreading ridge with average full spreading rates varying from 26 to 38 mm/yr. The disposition of the magnetic anomalies suggests that the plate opening direction has not changed during the last 0-4 Ma period. Along axis variations in the magnetic anomalies, presence of axial volcanic ridges on the inner valley floor, variations in the depth and geometry of the rift valley, suggest distinct variations in the accretionary processes along the ridge. Based on these characteristics and the segmentation pattern, we suggest that ten ridge segments are undergoing less magmatic phase of extension, while two segments have shown characteristics of magmatic accretion. The linear segments with narrow and shallow rift valley floor and near symmetric magnetic anomalies are identified as segments with magmatic accretion. The influence of diffuse plate boundary zone on the young seafloor fabric generated by the CIR has been examined. The seafloor topography different from the normal ridge parallel fabric observed at few places over the NE flank of the CIR is suggested to be the consequence of gradual and progressive influence of the distributed diffuse plate boundary (between the Indian-Capricorn plates), on the newly generated oceanic lithosphere. Further, we documented distinct ridge-transform intersection (RTI) highs, three of these RTI highs are identified as oceanic core complexes / megamullion structures. Megamullion structures are found to be associated with less magmatic sections. Increased seismicity has been observed at the less magmatic segment ends suggesting the predominance of tectonic extension prevalent at the sparsely magmatic sections.

Keywords: *Central Indian Ridge, Indian Ocean, multibeam bathymetry, magnetic anomalies, ridge segmentation, crustal accretion, megamullions, oceanic core complex*

1. Introduction

The Central Indian Ridge (CIR) north of the Indian Ocean triple junction is a slow spreading mid-ocean ridge in the Indian Ocean with full spreading rates less than 40 mm/yr. Basin scale regional marine geophysical investigations dealing with the tectonic evolution of the Indian Ocean (Vine and Matthews, 1963; McKenzie and Sclater, 1971; Schlich, 1982), and the plate reconstruction models (Royer et al. 1989; DeMets et al. 1994), have provided broad scale geometry of this ridge.

High-resolution mapping efforts over the mid-ocean ridges world-over revealed fine scale topographic fabric of the ridge crest region leading to the existence of new families of ridge axis discontinuities. These studies have shown that the ridge axis discontinuities primarily divide the ridge into smaller segments with varied topographic expressions as a consequence of crustal accretion resulting from discrete spreading cells (Macdonald and Fox, 1990; Shaw, 1992; Sinton and Detrick, 1992). The ridge systems in the north Indian Ocean are least explored with respect to surveys with modern mapping tools. Briaies (1995) and Kamesh Raju et al. (1997) provided initial results of detailed segment scale investigations carried out over parts of the CIR using modern tools such as Gloria side scan and multibeam bathymetry, respectively. The magnetic and bathymetric investigation results of Drolia et al. (2000) have provided tectonic implication of the ridge segmentation over a part of the CIR. Insights into the influence of diffuse plate deformation zone on the seafloor fabric and its implications were discussed (Drolia and DeMets, 2005) based on multibeam bathymetry and magnetic data. Some of these recent studies have been carried out under the Indian Ridge initiative coordinated by the National Institute of Oceanography, Goa, India and the National Geophysical Research Institute, Hyderabad, India. Swath bathymetry and magnetic data were acquired under this initiative to achieve complete coverage of the CIR from 3°S to 11°S over a 750 km-long section of the ridge. The resultant data provided high-resolution images of the ridge, highlighting the first and second order ridge segmentation and prominent ridge-transform intersection (RTI) highs.

The distinct topographic fabric of the ridge and its segmentation largely represent the temporal and spatial interplay of two primary accretionary processes, viz., i) magmatic process that provides the melt to form new oceanic crust, and ii) tectonic process during which deformation, faulting and dismemberment of the crust takes place. It is therefore, important to identify the contribution of these processes to understand the finer scale evolution of the ridge system. High-resolution geophysical data with off-axis coverage extending to few million years is required to understand the interplay between the magmatic and less magmatic (tectonic) processes that have affected the evolution of the

ridge segment. Extensive investigations carried out over East Pacific Rise (EPR) and over the segments of Mid-Atlantic Ridge (MAR) have provided insights into the segmentation pattern and accretionary processes of the fast and slow spreading ridge systems (Macdonald et al., 1991; Scheirer and Macdonald, 1993; Sempere et al., 1990, 1993; Smith et al., 1993; Gente et al., 1995; Goslin et al., 1999). Recent investigations over the ultra slow South West Indian Ridge (Sauter et al., 2001; Dick et al., 2003) and the Arctic Ridges (Cochran et al., 2003; Michael et al., 2003) have further enhanced our understanding on the architecture and accretionary processes of the slow spreading mid-ocean ridges.

In this paper, we present the first detailed analysis of the segmentation and morphology of the CIR between 3°S to 11°S based on multibeam bathymetry and magnetics. The across axis coverage of the multibeam survey has extended up to anomaly 3 (4 Ma).

2. Marine Geophysical Data

Newly acquired multibeam swath bathymetry and magnetic data during the 195 and 207 cruises of ORV Sagar Kanya (July 2003 and August 2004) are augmented with earlier published data of SK84 and SK165. All the multibeam data has been merged and re-processed. The data covers about 750 km long ridge with off-axis coverage of about 30 miles on either side of the spreading axis, 100% insonification of the seafloor was achieved by the 3 nautical mile spacing of the multibeam bathymetry tracks (Fig. 1). Total magnetic intensity data was acquired simultaneously with Geometrics marine magnetometer. Chain-bag dredge was used to collect rock samples. An Integrated Navigation System (INS) with GPS MX4400 as the primary control provided the navigation.

MB-System (Caress and Chayes, 1995) was used to process the multibeam bathymetry data. The total magnetic field data were reduced to anomaly by subtracting the IGRF filed model (IAGA, 2000). GMT (Wessel and Smith, 1991) software was used for plotting and presentation of the data.

Seafloor spreading magnetic model studies have been carried out to identify the magnetic anomalies and to assign the spreading rates. Synthetic anomaly profile is generated using the time scale of Cande and Kent (1995) and by assuming 500 m thick blocks with 4 A/m magnetization. The model studies suggest variable and asymmetric spreading rates ranging from 26 to 38 mm/yr.

3. Morphotectonic elements

The 750 km long section of the CIR is characterised by rugged topography, steep valley walls, and well defined rift valley floor, all characteristics of slow spreading ridges. The spreading rates are slightly higher than the slow spreading Carlsberg Ridge (Kamesh Raju et al., 2008) and the ridge is characterised by well defined spreading segments bounded by transform faults. The identified ridge segments are named from I to P and the corresponding fracture zones are labelled with a pre-fix “FZ-” to the segment name, following slightly modified notation from that of DeMets et al., (2005). In the present informal naming scheme, the fracture zone at the southern end of segment I is named as FZ-I and the fracture zone at the southern end of J is named as FZ-J and so on. Ridge segments separated by non-transform discontinuities are labelled with numbered alphabet (e.g. K1, K2, and M1, M2) (Figs. 1 and 2). A summary of the morphotectonic characteristics of the ridge segments identified in the present study is provided in Table 1.

3.1 Along axis variations

The along-axis depth profile with identified ridge segments, transform faults (TFs) and the non transform discontinuities (NTDs) is shown in figure 3a. The rift valley floor has an average depth of 3500 m and the along axis valley floor depth varied from 2743 m to 4638 m (Fig. 3). The segment L has the shallowest rift valley at 2743 m and is conspicuous in its character compared to other segments, the rift valley almost disappears at the center of this segment (Fig. 2). Excluding the segment L, the shallowest axial depth of each segment is in the range of 3500 - 4000 m. The maximum average measured full spreading rate of 38 mm/yr was observed over the segment L. Of the identified 12 segments majority of the segments have faster spreading rates over the north-eastern flank. There appears to be no apparent correlation between axial valley depth and the spreading rates (Fig. 3b).

Morphotectonic features of the identified ridge segments I to P (Fig. 4) are described in detail in the following sections. The average half spreading rate of each segment suggest asymmetric spreading in terms of spreading rate derived from magnetic model studies (Fig. 5) and the average full spreading rates varied from 26 to 38 mm/yr. The deepest portion of the transform valley reached a depth of 6300 m at the Vema transform.

3.2 Segment I

A limited part of segment I was mapped (Fig.4a). This segment is bounded in the north by the FZ-H and in the south by the Sealark fracture zone FZ-I. An expression of a non transform discontinuity (NTD) between FZ-H and FZ-I is seen on the satellite gravity map (Fig. 1). The surveyed part of the ridge is linear and is characterised by well defined ridge parallel topographic fabric. The rift valley width varied from 14 to 18 km. Well defined ridge parallel topographic fabric is observed on the flanks (Fig. 4a). Magnetic anomalies up to 2A have been identified and a half spreading rate of 14.0 mm/yr was ascribed based on magnetic model studies (Fig. 5).

3.3 Segment J

This segment is bounded by well defined transform faults FZ-I in the north and the FZ-J in the south. The segment is partially covered by multibeam survey and a small scale NTD exists towards southern end of the segment as expressed by the satellite gravity image (Fig. 1). Based on the partial multibeam coverage and the satellite gravity, this ridge section is further divided into J1, J2, and J3 (Figs. 1 and 2). A 62 km offset with segment I in the north and a 45 km offset in the south with segment K is observed. The rift valley width varied from 11 to 17 km and it is narrower than that of segment I. Configuration of the magnetic anomaly identifications indicates slightly asymmetric spreading with half spreading rates of 16.5 mm/yr on the western flank and 18.5 mm/yr on the eastern flank.

3.4 Segment K

The segment K is bounded on either side by well defined transform faults that characterise the fracture zones FZ-J and FZ-K (Vityaz fracture zone) in the north and south respectively. A well defined NTD further divides this ridge section into smaller segments K1 and K2. While the bounding transforms offset the ridge segments by 45 km and 100 km in the north and south respectively, the NTD offsets the ridge segments K1 and K2 by 15 km. The rift valley width varied from 10 to 14 km over K1 and it is about 24 km over the K2 (Fig.4a). Asymmetric spreading is noticed with 13.5 and 16 mm/yr half spreading rate across K1 and 13.5 and 17 mm/yr across the segment K2.

3.5 Segment L

The segment L is bounded on either side by well defined transform faults (Fig.4b) that offset the ridge axis by about 100 km and displays a completely different rift valley configuration. The valley

floor shallows to 2743 m at about 6°14' S and the rift valley disappears at this location. The rift valley is better defined toward segment ends where it is about 8 to 10 km wide. The half spreading rates varied from 19.3 mm/yr on the south-western flank to 18.5 mm/yr on the north-eastern flank, these are the fastest spreading rates measured along the investigated portion of the ridge. Well defined ridge parallel topographic fabric and magnetic lineations characterise this segment (Fig. 4b). A ridge transform intersection (RTI) high that shallows to a depth of 1600 m was noticed at the inside corner of the southern end of the ridge segment L (Fig. 2 and 4b).

3.6 Segment M

The segment M (Fig. 4c) is characterised by two minor segments M1 and M2 that are separated by a small offset (8 km) NTD. The segment is characterised by asymmetric spreading that is more prominent on M1 with varied spreading rates of 14.6 and 17.0 mm/yr (Fig. 5). The rift valley width varied from 15 to 18 km, well developed ridge parallel topographic fabric characterises the ridge segment.

3.7 Segment N

The segment N (Fig. 4c) is a linear ridge with well defined but relatively narrow rift valley of 8 to 15 km wide. The segment is offset by 64 km with respect to M2 in the north and is bounded in the south by the Vema transform fault that offsets the ridge axis by about 240 km. Half spreading rates of 15.0 mm/yr on the south-western flank to 15.5 mm/yr on the north-eastern flank indicate asymmetric spreading (Fig. 5). Ridge parallel topographic fabric is well developed.

3.8 Segment O

The segment O is 35 km long and is bounded by the 240 km long Vema transform fault in the north and 24 km long transform fault associated with FZ-O in the south (Fig. 4e). Symmetric spreading is observed with half spreading rate 13 mm/yr and has a narrow rift valley of less than 10 km wide. Vema transform represents one of the largest offset transform faults over the CIR (Drobia and DeMets, 2005).

3.9 Non - Transform Discontinuities

Two prominent non-transform discontinuities are documented encompassing the sections K1, K2, and M1, M2, these segments typically have wider and deeper rift valley floor with rugged and blocky flank topography. The NTD between K1 and K2 at 5°15'S offsets the ridge axis by about 15 km and

the rift valley floor widens to about 24 km across the segment K2. Oblique trending bathymetric lineations are observed towards north-eastern flank near to anomaly 2A (Fig. 4a). The non-transform fault between M1 and M2 at about 7°15'S has a smaller offset of ~ 8 km. Prominent axial volcanic ridges (AVRs) are observed over the rift valley floor (Fig. 4c). Based on the ridge-ridge offset between the segments and the presence of the off-axis trace, the NTD at 5°S separating K1 and K2 is classified as second order discontinuity while the NTD separating the M1 and M2 falls under the category of third order discontinuity (Macdonald et al., 1988). The absence of off-axis trace at this NTD suggests that it is relatively younger than the NTD at 5°S.

3.10 Ridge-Transform Intersection highs and Megamullion structures

Even though there are seven prominent RTI highs at the inside corners of the segments as seen on the bathymetry map (Fig. 2), only three of these features are recognised as Oceanic Core Complexes (OCCs) based on the diagnostic geomorphological characteristics defined by Tucholke et al. (1998). These OCCs, also called as megamullion structures are suggested to have formed due to the exhumation of mantle rocks through detachment faults. The identified megamullions in this study are named as m1 to m3 (Fig. 6). These are located near to the transforms that are bounded by sparsely magmatic ridge segments. The prominent dome shaped structures varied in length 35 to 39 km along the flow-lines parallel to the transform zone. We could observe prominent corrugations that align perpendicular to the ridge on m1 and m2 (Fig. 6a and 6b), these are less prominent on m3 (Fig. 6c). We have also relied on the dome-shaped feature, elongated along the relative plate motion flow-lines and the 3d-images of these structures to qualify them as megamullions. The lack of 100% coverage by the multibeam swaths at the shallow tops of these structures, probably, is making it difficult to identify the ridge-perpendicular corrugations.

An RTI high r1 (Fig. 2) that shallows to 1600 m is observed at the intersection of the segment J3 and the transform at about 4°48'S latitude. Another ridge transform intersection high r2 (Fig. 2) is observed at the NTD separating the segments K1 and K2, at 05°07'S latitude. This feature rises to 2000 m from the adjacent valley floor of 3800 m. Basalts and serpentized peridotites were recovered from the flank of this feature (Fig. 2 and Table 2).

The RTI high feature located at about 5°25'S latitude (Fig. 2) is identified as megamullion structure m1. This feature is at the inside corner of the southern end of the segment K2. It extends to about 39 km perpendicular to the ridge segment K2 and the shallowest portion of this OCC is at a depth of 1875 m (Fig. 6a). The shallow peak of this feature was earlier named as Kurchatov seamount in

some hydrographic maps. This feature was first identified as a megamullion structure by Drolia and DeMets (2005) and is known as Vityaz megamullion. Fresh basalts and serpentinized peridotites were recovered from dredge hauls over this megamullion structure (Fig. 6a).

A well developed inside corner high is noticed at the southern end of the segment L. This feature is identified as RTI high r3 (Fig. 2) and rises to about 1800 m from the adjacent seafloor deep of 4600 m. A prominent RTI high showing the characteristics of a megamullion structure is observed at the inside corner between segments L and M1 at about 7°08'S. This feature rises to about 1375 m from the RTI deep of 4300 m, and extends to about 34 km perpendicular to the ridge segment M1. This feature has been denoted as megamullion structure m2 (Fig. 6b).

A conspicuous RTI high r4 is observed on the inside corner of segment N at about 8°15' S (Fig. 2). The feature rises to a depth of < 2000 m from the adjacent RTI deep of 5000 m (Fig. 4c). Farther south at about 09° 27', a prominent megamullion structure is documented at the inside corner setup at the western end of the Vema transform fault on an older seafloor with respect to the ridge segment O. This structure shallows to 1620 m from the adjacent transform valley of 5000 m and is identified as megamullion structure m3 (Fig. 6c).

4. Magnetism

With few exceptions, the anomalies are well defined and correlatable. The amplitude of the central anomalies vary from 200 to 400 nT with about 100 nT local highs and lows in the middle (Fig. 5), corresponding to the neo volcanic zone along the rift valley floor. These signature changes are probably the reflection of the magnetization variations within the crust. Magnetic anomalies up to 2A have been identified throughout the ridge section and anomaly 3 was seen along the profiles crossing segments N and O (Fig. 5). The identified magnetic anomalies depict good agreement with the bathymetric lineation pattern and rift valley configuration (Fig. 4). The asymmetry observed in the spreading rate is discernable on the topographic fabric and is prominent along the ridge segments bounded by the NTDs. Oblique bathymetric lineations are observed over the eastern flank of segment K1 around 5° S; however, the magnetic lineations corresponding to anomaly 2A in this region appear to be ridge parallel (Fig. 4a). The off axis trace of the NTD is seen extending till anomaly 2A suggesting that the NTD has existed since anomaly 2A time. However, the off-axis trace of the NTD between the segments M1 and M2 around 7°30'S is not significant (Fig. 4c). While the axial geometry is related to the local magma supply variations, there is no apparent correlation

between the along axis depth variations and the inferred spreading rates (Fig. 3). The finer variations observed in the spreading rates are attributed to local changes.

The inferred full spreading rates varied from 26 to 38 mm/yr. We have also computed the spreading rates using the MORVEL model (DeMets et al., 2010). For these computations we have used Somalia-Capricorn plate pair for segment O, and for the segments north of Vema transform we have used Africa-India (Somalia-India) plate pair following Drolia and DeMets (2005). These results are summarised in Table 1. The spreading rates derived from the MORVEL model varied from 32 to 35 mm/yr and are comparable to the measured rates obtained from seafloor spreading model studies using the marine magnetic data (Fig. 3b). The rates derived from the MORVEL model increase linearly as the distance from the pole to the observational point increases. However, the measured full rates do not show systematic linear increase but vary from segment to segment.

5. Discussion

The 750 km long section of the CIR has a segmentation pattern that is similar to the slow spreading MAR with comparable spreading rates. The disposition of the magnetic anomalies suggests that the plate opening direction has not changed during 0-4 Ma period. This observation agrees well with independent kinematic evidence for steady state opening rates across the CIR and Carlsberg Ridges (DeMets et al., 1994, 2005) and the analysis of multibeam data (Drolia and DeMets, 2005). More recent evidence for steady spreading rates across the northern Central Indian Ridge suggest that changes in the opening rates during the past 7 Ma are less than 2 percent (Merkouriev and DeMets, 2006 and Bull et al., 2010). Prominent non-transform discontinuities are observed for the first time over two sections of the CIR. Seabed sampling along the ridge recovered mostly fresh basalts along the rift valley floor and flanks, mantle rocks were recovered at three RTI highs. Table 2 summarises the lithological characters of the seabed samples. The ridge segmentation and nature of accretion along the ridge segments, influence of the diffuse plate boundary on the fine scale tectonics of the ridge, identification of OCCs / megamullion structures, and inferences from observed seismicity are the major elements that are highlighted in the present study. These aspects are discussed in detail in the following sections.

5.1 Magmatic and less-magmatic segments

The multibeam bathymetry data over the surveyed section of the CIR has shown wide variation over the along axis and across axis morphotectonic character within and between the ridge segments. These variations are similar to the northern and southern MAR and the Carlsberg Ridge segments

(Karson et al., 1987; Grindlay et al., 1992; Fox et al., 1991; Sempere et al., 1993; Kamesh Raju et al., 2008). The studies of ridge crest morphology over the slow spreading ridges have shown that there is discernable relationship between the rift valley morphology and the crustal accretionary and extensional processes. Based on extensive study of the ridge crest morphologies it was suggested that the rift valley morphologies are a consequence of competing magmatic and tectonic (less magmatic extension) processes and are related to magma supply (Perfit and Chadwick, 1998). Segments with narrow and shallow V-shaped rift valley are interpreted to be magmatic and this interpretation is supported by the presence of circular mantle Bouguer anomaly lows observed over these ridge segments indicating focused mantle upwelling resulting in thicker crust (Kuo and Forsyth, 1988; Lin et al., 1990; Tolstoy et al., 1993; Fujimoto et al., 1996; Maia and Gente, 1998). The ridge segments with deeper and wider U-shaped valley configuration with rough topographic fabric are considered to be sparsely magmatic with dominant tectonic extension. Based on these criterion, the ridge segments in the present study are classified as magmatic and less magmatic segments.

There are two sections that encompass non-transform discontinuities bounding the segments K1, K2 and M1, M2. These sections appear to be less magmatic with rugged flank topography, deep and wide rift valley floor (Fig. 4a and 4c), and disturbed magnetic signature (Fig. 5, segment M1). Oblique abyssal hill fabric is noticed at 5°S on the NE flank of the segment K1 (Figs. 2 and 4a). The oblique trending fabric is prominent beyond anomaly 2A. Oblique trending fabric is also noticed on the NE flank of the segment M1 (Figs. 2 and 4b). The abyssal hill pattern could be a consequence of less magmatic tectonic extension along these two segments that are also characterised by NTDs

Segments L and N display characteristics of magmatic sections. The segment L has the shallowest valley floor reaching to 2743 m in the middle of the segment, suggesting thicker crust due to local upwelling of magma. The Segment N displays well defined ridge parallel topographic fabric. A relative mantle Bouguer anomaly (MBA) low observed in the middle of this segment was suggested to be the consequence of crustal accretion due to magmatic activity (Kamesh Raju et al., 1997).

The segment N is bounded in the south by the prominent Vema transform fault that offsets the ridge axis by about 240 km. The Vema transform is one of the deepest portions of the Indian Ocean region documenting a depth of about 6300 m. This transform probably is affected by excess stretching and thinning of the crust in response to the plate motion. Short ridge segments (Segments O and P, Fig. 2) separated by transform faults are observed south of the Vema transform. These short segments are probably the result of sparse magmatic activity.

The overall segment lengths varied from 18 to 75 km, the shortest is segment O and the longest being the segment L with shallow rift valley floor. Segments L and N have narrow and shallow rift valleys and have lengths of 75 km and 60 km respectively. The segments L and N can be suggested to be undergoing magmatic phase of accretion based on similarities in the topographic fabric, rift valley morphology, and the presence of mantle Bouguer anomaly low over segment N (Kamesh Raju et al., 1997). The segments I, J, K, M, and O characterised by well defined wide rift valleys with deep valley floor that varied between 3500 to 4500 m appear to be experiencing less magmatic or sparsely magmatic phase of accretion.

The manifestation of the effect of magma supply over the rift valley morphology is conspicuous on the slow spreading ridges that are supported by discrete cells of focussed magma supply zones, in contrast to uniform crustal thickness over the fast spreading ridges (Lin and Morgan, 1992; Tolstoy et al., 1993). The occurrence of focussed magma upwelling zones as indicated by the MBA lows, greatly influence the topographic character of the ridge segments. Combination of the magmatic and less magmatic processes result in ridge segments that are highly variable in terms of rift valley morphology and the ridge flank topographic fabric. Such characterisation is discernable on the surveyed section of the CIR. It is also observed that magmatic segments are associated with well defined transform faults while the less magmatic sections are often associated with NTDs. The NTDs are non-steady state features that are spatially and temporally variable (Macdonald et al., 1988; Spencer et al., 1997) and respond to changes in melt driven processes. The magmatic influx of both the segments of the NTD is independently modulated and results in the lengthening of the more magmatic segment at the expense of the less magmatic segment (Gac et al., 2006).

5.2 Influence of Indian Ocean diffuse plate boundary on CIR

The study region falls within the broad diffuse plate boundary zone that extends from the CIR to Sumatra trench in the equatorial Indian Ocean, this diffuse plate boundary separates the Indian and Capricorn plates (Wiens et al., 1985; Gordon et al., 1990; Royer and Chang, 1991; DeMets et al., 1994; Royer et al., 1997). The region east of the CIR between 3°S and 11°S in particular falls within the diverging zone of the diffuse plate boundary (Gordon et al., 1990; DeMets et al., 1994; Royer et al., 1997; Gordon et al., 1998). The southern boundary of this domain coincides with the Vema transform fault (Royer et al., 1997; Drolia and DeMets, 2005) and the northern boundary coincides with the fracture zone FZ-H (DeMets et al., 2005). The NTD identified at about 5°30'S in the present study was earlier marked as disturbed fabric (Drolia and DeMets, 2005) due to partial multibeam coverage. At around 5°S we have noticed oblique trending abyssal hill fabric beyond

anomaly 2A (~ 3.5 Ma), on the eastern flank of the CIR suggesting the influence of Indian Ocean deformation zone. The suggested N-S divergence (Royer and Gordon, 1997) for the past 11 Ma and the present day NE spreading direction of the CIR may induce a component of counter-clockwise rotation of lithospheric blocks in the region of the extensional domain. The oblique abyssal hill orientations observed on the NE flank are probably indicative of such rotational effect. Changes in the seafloor fabric different from the normal ridge parallel fabric are observed at places corresponding to the NE flank regions of segments K1, K2, L, M1 and M2 (Figs. 2, 4a, 4b and 4c) with varying degree of obliqueness. They are more prominent on the NE flank of the segments K1, K2, less prominent over the segments M1 and M2 and only a feeble expression is seen over the NE flank of segment L. The effect of diffuse plate boundary on the seafloor spreading process and consequently on the seafloor fabric is not obvious in the multibeam data except probably over the segments K1 and K2. This may be due to two possible reasons. Either we have less off-axis coverage over the other segments or the deformation is not uniformly distributed within the delineated zone. We interpret the oblique abyssal hill fabric observed on the NE flank regions of the segments K1, K2 as the resultant effect of the component of N-S divergence and the NE spreading of the seafloor. The reasons for the absence of such distinct bathymetric fabric on the NE flanks of the other segments are not clear. It is probable that the component of N-S divergence may not be uniform throughout the deformation zone. This observation agrees well with the Drolia and DeMets (2005) model that suggest gradual rotation of lithosphere blocks within the deformation zone at rates that increase across the zone.

5.3 Oceanic Core Complexes

Three prominent megamullion structures representing oceanic core complexes have been suggested on the investigated section of the CIR at the inside corners of the RTIs (Fig. 2). These megamullion structures are observed at both transform and non-transform discontinuities. It is seen that megamullion structures are well developed near the transforms bounded by less magmatic sections of the ridge. This observation suggests that phases of amagmatic extension facilitate the slip along the detachment fault and intrusion of magma leading to the formation of megamullion structures, as seen along the sections of MAR (Tucholke et al., 1998). The spreading rates of the segments encompassing the megamullion structures varied from 26 to 31 mm/yr. These spreading rates broadly fall in the window of most common spreading rates encompassing the megamullion structures in the world oceans (Tucholke et al., 2008). Fresh basalts and serpentinized peridotites (Table 2) were recovered over the megamullion structures. Presence of serpentinites at the

megamullion structure m1 indicates mantle derived material. The exposure of peridotites indicative of upper mantle rocks implies thin crust and moderate supply of magma.

5.4 Seismicity

Higher levels of seismicity as evidenced by the increased number of teleseismic events are seen (Fig. 1) at the RTIs with well developed megamullion structures. Clustering of earthquake events of higher magnitude range (M_w 5 to 7) are observed at segments K2, M1 and off-axis of segment O (Fig. 1), these clusters coincide with the occurrence of suggested megamullion structures m1, m2 and m3 respectively. The increased seismicity may be due to the fluid circulation along the detachment fault. This observation supports the idea that the detachment faults associated with the megamullion structures are active and promote fluid circulation (Escartin et al., 2008). Increased seismicity at the less magmatic segment ends suggests predominance of tectonic extension prevalent at the sparsely magmatic sections; this in turn could have promoted the development of megamullion structures. The other place of high seismicity along the surveyed section of the CIR is at the Vema transform region at 9°S. The present data provides near full coverage of the Vema transform fault. Extensive block movements are seen along the transform and a megamullion feature is seen on the older seafloor corresponding to the segment O. It was suggested that the present southern limit of the diffuse plate boundary coincides with the Vema FZ (Drobia and DeMets, 2005). The increased seismicity at this place may be a consequence of the interaction of diffuse plate boundary with the Capricorn plate.

6. Conclusions

The segmentation of the CIR is marked by the transform and non-transform discontinuities. Two prominent NTDs and seven well defined transform faults define the segmentation of the CIR. Combination of the magmatic and less magmatic processes resulted in the ridge segments that are highly variable in terms of rift valley morphology and the ridge flank topographic fabric on the surveyed section of the CIR. It is also observed that magmatic segments are associated with well defined transform faults while the less magmatic sections are often associated with NTDs.

The average full spreading rates derived from the seafloor spreading model studies varied from 26 to 38 mm/yr. These rates are comparable to the slow spreading MAR and Carlsberg Ridges and the spreading rates derived from the MORVEL model.

Changes in seafloor fabric different from the normal ridge parallel fabric observed at few locations on the NE flank of the CIR are suggested to be the consequence of gradual and progressive influence of the N-S divergence component of the distributed diffuse plate boundary between the Indian-Capricorn plates on the newly generated oceanic lithosphere. This inference implies that the influence of the N-S divergence component of the diffuse plate boundary is not uniform in the entire zone.

Three prominent megamullion/OCC structures have been suggested after screening seven RTI high features identified over the surveyed section of the CIR. It is observed that the megamullion structures are located on less magmatic segments of the ridge.

Acknowledgements

We thank Dr. S.R. Shetye, Director, National Institute of Oceanography, Goa, for the encouragement and support given to carry out the study. We thank Dr. Jerome Dymant, an anonymous reviewer, and Dr. DeMets for providing useful suggestions and comments on this paper. Comments and suggestions, in particular by Jerome Dymant and DeMets helped us to improve the manuscript. Editor-in-Chief, Dr. Hans Thybo is thanked for suggestions and encouragement. The study was carried out under the CSIR Network program on RIDGES and the MoES funded Hydrothermal Sulphides program. Ministry of Earth Sciences (MoES), New Delhi is thanked for providing ship time on ORV Sagar Kanya. This is N.I.O. contribution no. XXXX.

References

- Briaies, A., 1995. Structural analysis of the segmentation of the Central Indian Ridge between 20°30' and 25°30' S (Rodriguez Triple Junction). *Mar. Geophys. Res.* 17, 431–467.
- Bull, J.M., De Mets, C., Krishna, K.S. and Sanderson, D.J., 2010. Reconciling lithospheric convergence in the central Indian Ocean determined from plate kinematics and seismic reflection data. *Geology*, 38, (4), 307-310, doi:10.1130/G30521.1
- Cande S.C., Kent D.V., 1995. Revised calibration of the geomagnetic polarity timescale for the late Cretaceous and Cenozoic. *J. Geophys. Res.* 100, 6093-6095.
- Caress, D.W., Chayes, D.N., 1995. MB-system, Developed at Lamont–Doherty Earth Observatory Report.
- Cochran, J.R., Kurrus, G.J., Edwards, M.H., Coakley, B.J., 2003. The Gakkel Ridge: Bathymetry, gravity anomalies and crustal accretion at extremely slow spreading rates. *J. Geophys. Res.* 108, doi: 10/1029/2002JB001830.
- DeMets, C., Gordon, R. G., and Royer, J.-Y., 2005. Motion between the Indian, Capricorn, and Somalian plates since 20 Ma: Implications for the timing and magnitude of distributed lithospheric deformation in the equatorial Indian Ocean. *Geophys. J. Int.* 161, 445–468.

- DeMets, C., Gordon, R. G., and Vogt, P., 1994. Location of the Africa-Australia-India triple junction and motion between the Australian and Indian plates: Results from an aeromagnetic investigation of the Central Indian and Carlsberg ridges. *Geophys. J. Int.*, 119, 893–930.
- DeMets, C., Gordon, R.G., Argus, D.F., 2010. Geologically current plate motions. *Geophys. J. Int.*, 181, 1 - 80.
- Dick, H.J.B, Lin, J., Schouten, H., 2003. An ultraslow- spreading class of Ocean ridge. *Nature* 426, 405-412.
- Droliia, R. K., and DeMets, C., 2005. Deformation in the diffuse India-Capricorn-Somalia triple junction from a multibeam and magnetic survey of the northern Central Indian ridge, 3°S–10°S. *Geochem. Geophys. Geosyst.* 6, Q09009, doi: 10.1029/2005GC000950.
- Droliia, R. K., Ghose, I., Subramanyam, A. S., Malleswara Rao, M. M., Kessarkar, P., and Murthy, K. S. R., 2000. Magnetic and bathymetric investigations over the Vema Region of the Central Indian Ridge: Tectonic implications. *Mar. Geol.* 167, 413–423.
- Escartin J., D.K. Smith, J.R. Cann, H. Schouten, C.H. Langmuir, and S.Escrig., 2008. Central role of detachment faults in accretion of slow spreading oceanic lithosphere. *Nature* 455, 790-794, doi:10.1038/nature07333.
- Fox, P.J., Grindlay, N.R., and Macdonald K.C., 1991. The Mid-Atlantic Ridge (31°S-34°30'S): Temporal and spatial variations of accretionary processes. *Mar. Geophys. Res.* 13, 1-20.
- Fujimoto, H., Seama, N., Lin, J., Matsumoto, T., Tanaka, T., and Fujioka, K., 1996. Gravity anomalies of the Mid-Atlantic Ridge north of the Kane Fracture Zone. *Geophys. Res. Lett.* 23, 3431-3434.
- Gac, S., Tisseau, C., Dymont, J., and Goslin, J., 2006. Modelling the thermal evolution of slow-spreading ridge segments and their off-axis geophysical signature. *Geophys. J. Int.* 164, 341-358.
- Gente, P., Pockalny, R.A., Durand, C., Deplus, C., Maria, M., Ceuleneer, G., Mevel, C., Cannet, M., Laverne, C., 1995. Characteristics and evolution of the segmentation of the Mid-Atlantic Ridge between 20°N and 24°N during the last 10 million years. *Earth Planet. Sci. Lett.* 129, 22-71.
- Gordon, R.G., DeMets, C., and Argus, D.F., 1990. Kinematic constraints on distributed lithospheric deformation in the equatorial Indian Ocean from present motion between the Australian and Indian plates. *Tectonics* 9, 409-422.
- Goslin, J., Triatnord Scientific party, 1999. Extent of Azores plume influence on the Mid-Atlantic Ridge north of hotspot. *Geology* 27, 991-994.
- Grindlay, N.R., Fox, P.J., and Vogt, P.R., 1992. Morphology and tectonics of the Mid-Atlantic Ridge (25°-27°30'S) from SeaBeam and magnetic data. *J.Geophys. Res.* 97, 6983-7010.
- Kamesh Raju, K.A., Chaubey, A.K., Dileep Amarnath., Abhay Mudholkar., 2008. Morphotectonics of the Carlsberg Ridge between 62°20' and 66°20'E, northwest Indian Ocean. *Mar. Geol.* 252, 120-128.
- Kamesh Raju, K.A., Ramprasad, T., Subrahmanyam, C., 1997. Geophysical investigations over a segment of the Central Indian Ridge, Indian Ocean. *Geo-Mar. Lett.* 17, 195-201.

- Karson, J.A., 1987. Along-axis variations in seafloor spreading in the MARK area. *Nature* 328, 681-685.
- Kuo, B.Y., and Forsyth, D.W., 1988. Gravity anomalies of the ridge-transform system in the south Atlantic between 31 and 34.5°S: Upwelling centers and variations in crustal thickness. *Mar. Geophys. Res.* 10, 59-90.
- Lin, J., and Morgan, J.P., 1992. The spreading rate dependence of three-dimensional mid-ocean ridge gravity structure. *J. Geophys. Res. Lett.* 19, 13-16.
- Lin, J., Purdy, G.M., Schouten, H., Sempere, J.C., and Zervas, C., 1990. Evidence from gravity data for focused magmatic accretion along the Mid-Atlantic Ridge. *Nature* 344, 627-632.
- Macdonald, K.C., Fox, P.J., Perram, L.J., Eisen, M. F., Haymon, R.M., Miller, S.P., Carbotte, S.M., Cormier, M. H., and Shor, A.N., 1988. A New View of the Mid-Ocean Ridge From the Behaviour of Ridge Axis Discontinuities. *Nature* 335, 217-225.
- Macdonald, K.C., Fox, P.J., 1990. Mid Ocean Ridge. *Sci. Am.* 262 (no.6), 42-49.
- Macdonald, K.C., Scheirer, D.S., Carbotte, S.M., 1991. Mid-Ocean Ridge: Discontinuities, Segments and Giant Cracks, *Science* 253, 986-994.
- Maia, M and Gente, P., 1998. Three-dimensional gravity and bathymetry analysis of the Mid-Atlantic Ridge between 20°N and 24°N: Flow geometry and temporal evolution of the segmentation. *J. Geophys. Res.*, 103, 951-974.
- Merkouriev, S., DeMets, C., 2006. Constraints on Indian plate motion since 20 Ma from dense Russian magnetic data: implications for Indian plate dynamics. *Geochem. Geophys. Geosyst.* 7, Q02002, doi: 10.1029/2005GC001079.
- McKenzie, D.P., Sclater, J.G., 1971. The evolution of the Indian Ocean since the Late Cretaceous. *Geophys. J. R. Astron. Soc.* 25, 437-528.
- Michael, P.J., Langmuir, C.H., Dick, H.C.B, Snow, J.E., Goldstein, S.L., Grraham, D.W., Lehnert, K., Kurras. G., Jokat, W., Muhe, R., Edmonds, H.N., 2003. Magmatic and amagmatic seafloor generation at the ultraslow-spreading Gakkel ridge, Arctic Ocean. *Nature* 423, 956-961.
- Perfit, M.R., and Chadwck Jr, W.W., 1998. Magmatism at mid-ocean ridges: Constraints from volcanological and geochemical investigations, in: Roger Buck, W., Delaney, T. Paul., Karson, A. Jeffrey, and Lagabrielle, Yves, (Eds.), *Faulting and Magmatism at Mid-Ocean Ridges. Geophysical Monograph 106*, American Geophysical Union, Washington, pp. 59-115.
- Royer, J.Y., Sandwell, D.T., 1989. Evolution of the eastern Indian Ocean since the Late Cretaceous - Constraints from Geosat altimetry. *J. Geophys. Res.* 94, 13755-13782.
- Royer, J.Y., and Chang, T., 1991. Evidence for relative motions between the India and Australian plates during the last 20 Myr from plate tectonic reconstruction: Implications for the deformation of the Indo-Australian plate. *J. Geophys. Res.* 96, 11779-11802.
- Royer, J.Y., Gordon, R.G., 1997. The Motion and Boundary between the Capricorn and Australian Plates. *Science*, 277, 1268-1274.
- Sandwell, D.T, Smith, W.H.F., 1997. Marine gravity anomaly from geosat and ERS-1 altimetry, *J. Geophys. Res.* 102, 10039-10054.

- Sauter, D., Partriat, P., Jestin, C.R., Cannet, M., Brias, A., Gallieni Shipboard Scientific Party, 2001. The Southwest Indian Ridge between 49°15'E and 57°E: focused accretion and magma redistribution. *Earth Planet. Sci. Lett.* 192, 303-317.
- Scheirer, D.S., Macdonald, K.C., 1993. Variation in cross-sectional area of the axial ridge along the East Pacific Rise: Evidence for the magmatic budget of a fast spreading center. *J. Geophys. Res.* 98, 7871-7885.
- Schlich, R., 1982. The Indian Ocean: Aseismic ridges, spreading centers, and oceanic basins, in: A. E. M. Nairn and F. G. Stehli, (Eds.), *The Ocean Basins and Margins*. vol. 6, The Indian Ocean, Plenum, New York, pp. 51-147.
- Sempere, J.C., Lin, J., Brown, H.S., Schouten, H. Purdy, G.M., 1993. Segmentation and Morphotectonic variations along a Slow –Spreading Center: The Mid-Atlantic Ridge (24°00'N-30°40'N). *Mar. Geophys. Res.* 15, 153-200.
- Sempere, J.C., Purdy, G.M., Schouten, H., 1990. The segmentation of the Mid-Atlantic Ridge between 24°N and 30°40'N. *Nature* 344, 427-431.
- Shaw, P.R. 1992. Ridge segmentation, faulting and crustal thickness in the Atlantic ocean. *Nature* 358, 490-493.
- Sinton, J. M., Detrick, R. S., 1992. Mid-Ocean Ridge Magma Chambers. *J. Geophys. Res.* 97, 197–216.
- Smith, D.K., Cann, J.R.. 1993. Building the Crust at the Mid-Atlantic Ridge. *Nature* 365, 707-715.
- Spencer, S., Smith, D.K., Cann, J.R., Lin, J., and Mcallister, E., 1997. Structure and Stability of Non-Transform Discontinuities on the Mid-Atlantic Ridge between 24°N and 30°40'N. *Mar. Geophys. Res.* 19, 339-362.
- Tolstoy, M., Harding, A. J., and Orcutt, J.A., 1993. Crustal Thickness on the Mid-Atlantic Ridge Bull's Eye Gravity Anomalies and Focused Accretion. *Science* 262, 726-729.
- Tucholke, B.E., Behn, M.D., Buck, R.W., Lin, J. 2008. Role of melt supply in oceanic detachment faulting and formation of megamullions. *Geology*, 36, 455-458.
- Tucholke, B.E., Lin, J., Kleinrock, M.C., 1998. Megamullion and mullion structures defining oceanic metamorphic core complexes on the Mid-Atlantic Ridge. *J. Geophys. Res.* 103, 9857-9866.
- Vine, F. J., Matthews D M., 1963. Magnetic anomalies over ocean ridges. *Nature* 199, 947 949.
- Wessel, P., Smith, W.H.F., 1991. Free software helps map and display data, *Eos Trans. AGU* 72, 445–446.
- Wiens, D.A., 1985. A diffuse plate boundary model for Indian Ocean tectonics. *Geophys. Res. Lett.* 12, 429-432

Figure legends

Figure 1. Ship tracks, identified ridge segments, fracture zones, earthquake epicentres from the NEIC catalogue plotted on satellite gravity (Sandwell and Smith, 1997). Thick track lines indicate the selected profiles on each segment for magnetic model study (Fig. 5). Multibeam bathymetry is shown in light shade. The boxes a to e refer to the detailed maps shown in Figure 4a to 4e. Inset shows the Indian Ocean Ridge system along with the broad deformation zone (DeMets et al., 1994), the shaded regions with red and blue outlines within the deformation zone represent the divergent and convergent domains (Royer and Gordon, 1997) respectively.

Figure 2. Multibeam bathymetry over the CIR. Numbered green and red square symbols denote the dredge sampling locations, green indicates fresh basalts and red indicates recovery of mantle derived rocks. Numbers refer to samples listed in Table 2. m1, m2 and m3 indicate the identified megamullion features. r1, r2, r3, r4 indicate ridge-transform intersection highs. Other elements are same as in Figure 1.

Figure 3. a. Along axis depth profile and b. Average full spreading rate, half spreading rates over the south-western and north-eastern flanks of the ridge segments and the predicted spreading rates computed from MORVEL model (DeMets et al., 2010). TF indicates transform fault and NTD indicates the non-transform discontinuity.

Figure 4. Detailed multibeam bathymetry maps along with identified magnetic anomalies, transform faults and fracture zones. FZ represents fracture zone and AVR denotes axial volcanic ridges. Contours in blue with tick marks represent bathymetry lows and the red contours represent highs. Figures 4a, 4b, 4c, 4d, and 4e refer to the boxes a to e on Fig. 1.

Figure 5. Seafloor spreading magnetic models for selected profiles over each segment. The segment names are indicated. The average half spreading rate in mm/yr on each flank is indicated by numbers in brackets. Thick line indicates observed anomaly.

Figure 6. Megamullion structures identified at the inside corners. a-c represent the detailed multibeam bathymetry and the profile plot across the suggested megamullion structures m1, m2 and m3, identified across the segments K2, M1 and O respectively. Ridge axis and transform faults are indicated by thick red and black lines respectively. Seabed sample locations are indicated by square symbol. BA and T on the profile plot indicate breakaway and termination zones (Tucholke et al., 1998) respectively.

Table 1: Characteristics of ridge segments – Central Indian Ridge (3°S to 11°S)

Segments	Axial valley width km	Segment Length km	Offset between ridge segments (km), and the type (TF/NTD)	Measured full spreading rate mm/yr.	Full spreading rate mm/yr. MORVEL model.	Comments
I	14-18	19.65	61.2, TF	27.00	32.4	--
J	11-17	39.82		49.2, TF	35.00	32.6
K1	10-14	23.60	19.2, NTD	29.50	32.9	Presence of RTI high (r2) at the inside corner.
K2	24	18.83		108, TF Vityaz	30.50	33.0
L	8-10	74.46	92, TF	37.83	33.3	Prominent RTI high (r3).
M1	18	15.66		13.4, NTD	31.67	33.4
M2	15-18	21.93	64.4, TF	34.50	33.5	No RTI high.
N	8-15	60.00		243, TF Vema	30.50	33.8
O	15	18.14		26.00	35.2	A high on the older seafloor along the transform resembles OCC m3.

Characteristic features of the ridge segments. TF denotes transform fault and NTD is non-transform discontinuity. RTI is ridge transform intersection. Axial valley width is considered as the width between the 3000 m depth contours with the exception of segment L, where the valley shallows to less than 3000 m. Ridge-transform highs r1-r4 and OCC/Megamullion structures m1-m3 are indicated in Figure 2. Measured spreading rates are obtained from the seafloor spreading model studies and the predicted spreading rates are from MORVEL model (DeMets et al., 2010). Somalia and Capricorn plate pair was used for the segment O and Somalia – India plate pair was used for the segments north of Vema transform for the computation of spreading rates using MORVEL.

Table 2. Brief description of lithology of rocks recovered. The sample locations are numbered from north to south (see figure 2 for location on map).

Sr. no	Latitude (S)	Longitude (E)	Depth (m)	Lithology
1.	05° 11.021'	68° 28.101'	2999	Basalts (ropy & massive), serpentized peridotites, gabbro (1, 2, 7, and 9).
2.	05° 26.978'	68° 31.755'	2258	
3.	05° 29.756'	68° 13.423'	2470	
4.	06° 03.047'	68° 29.865'	2362	Variety of basalts, e.g. with glass cover, pillow, ropy, columnar, altered, oxide encrusted (3 to 6, 8, 10, 11, 13, and 14).
5.	06° 20.077 '	68° 17.509'	3573	
6.	06° 32.639'	67° 59.062'	3070	
7.	06° 38.506'	68° 19.340'	2700	
8.	07° 06.531'	68° 06.406'	1560	Massive basalts with column structure, volcanic breccia (12).
9.	07° 49.370'	68° 03.800'	1763	
10.	07° 59.340'	68° 01.150'	3634	
11.	08° 58.970'	67° 14.270'	2242	
12.	09° 27.400'	66° 58.240'	1735	
13.	09° 45.420'	66° 36.960'	3245	
14.	09° 53.640'	66° 35.720'	2000	

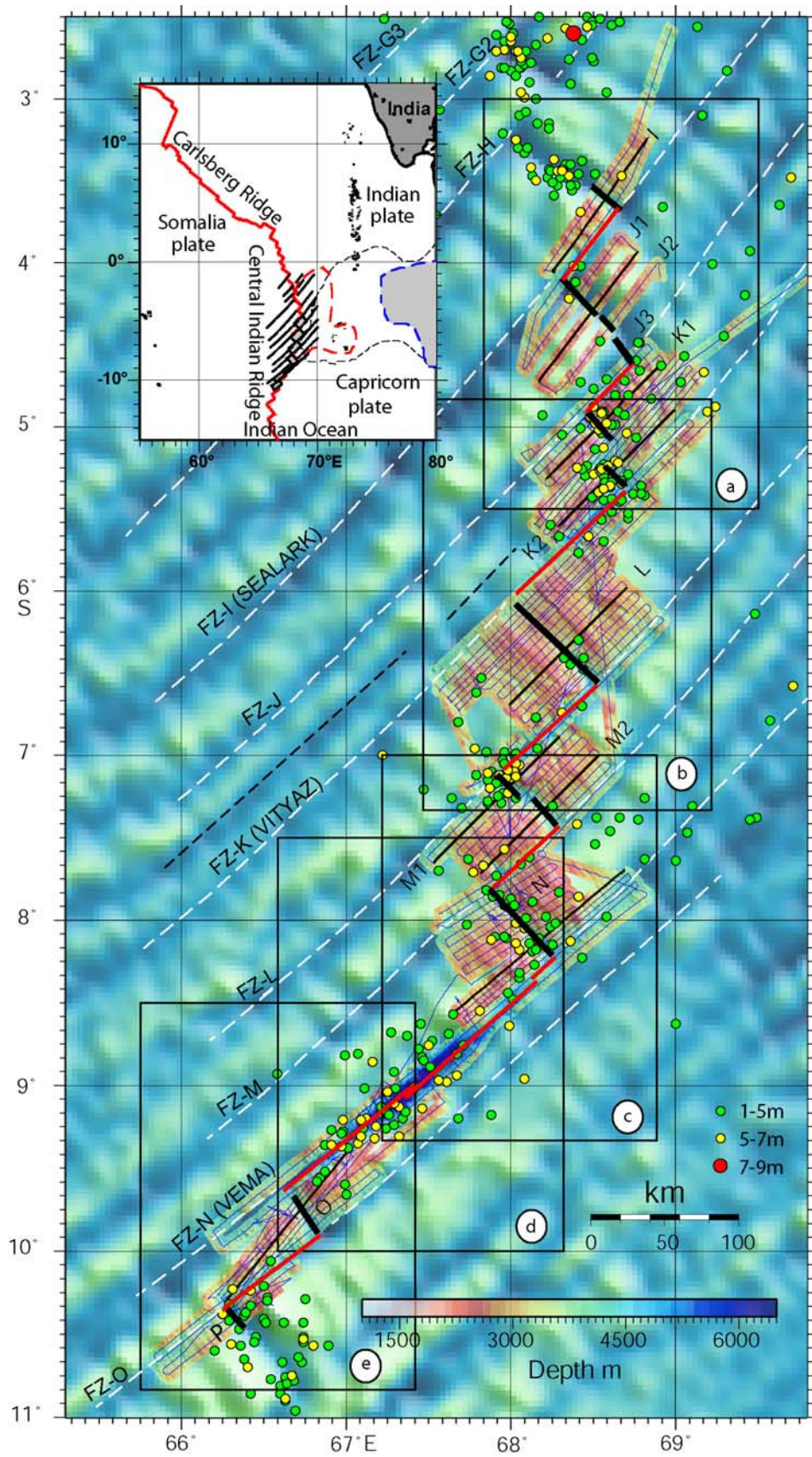


Figure 1

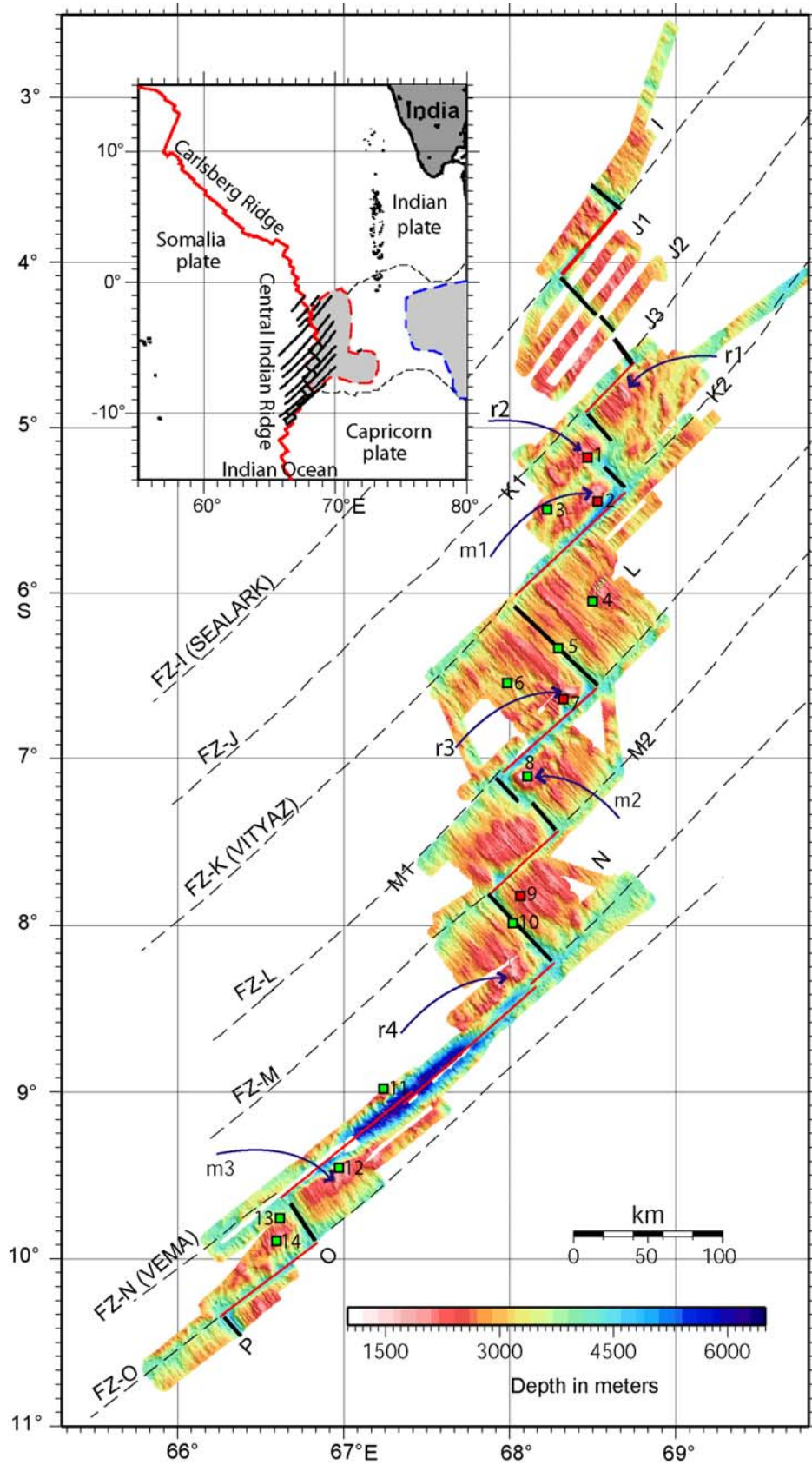


Figure 2

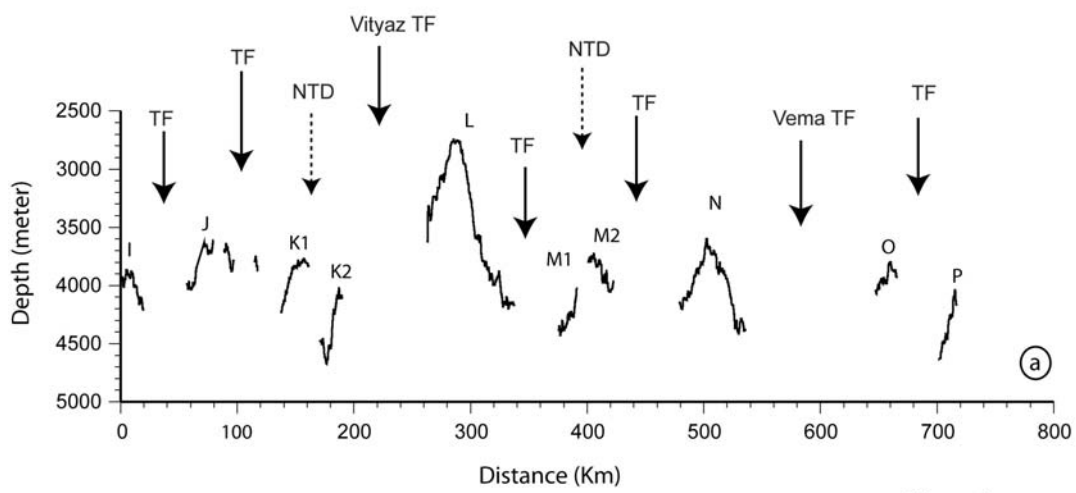
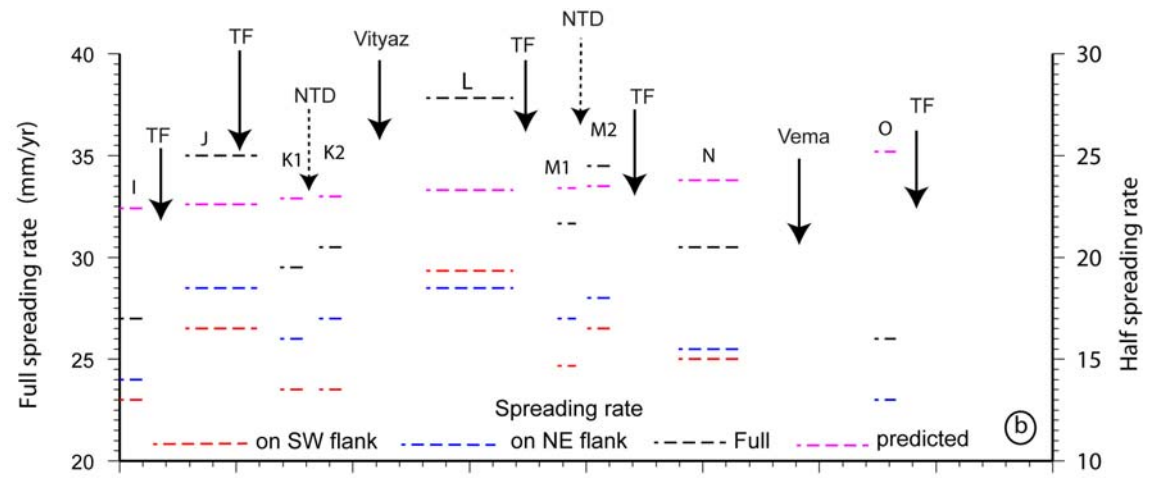
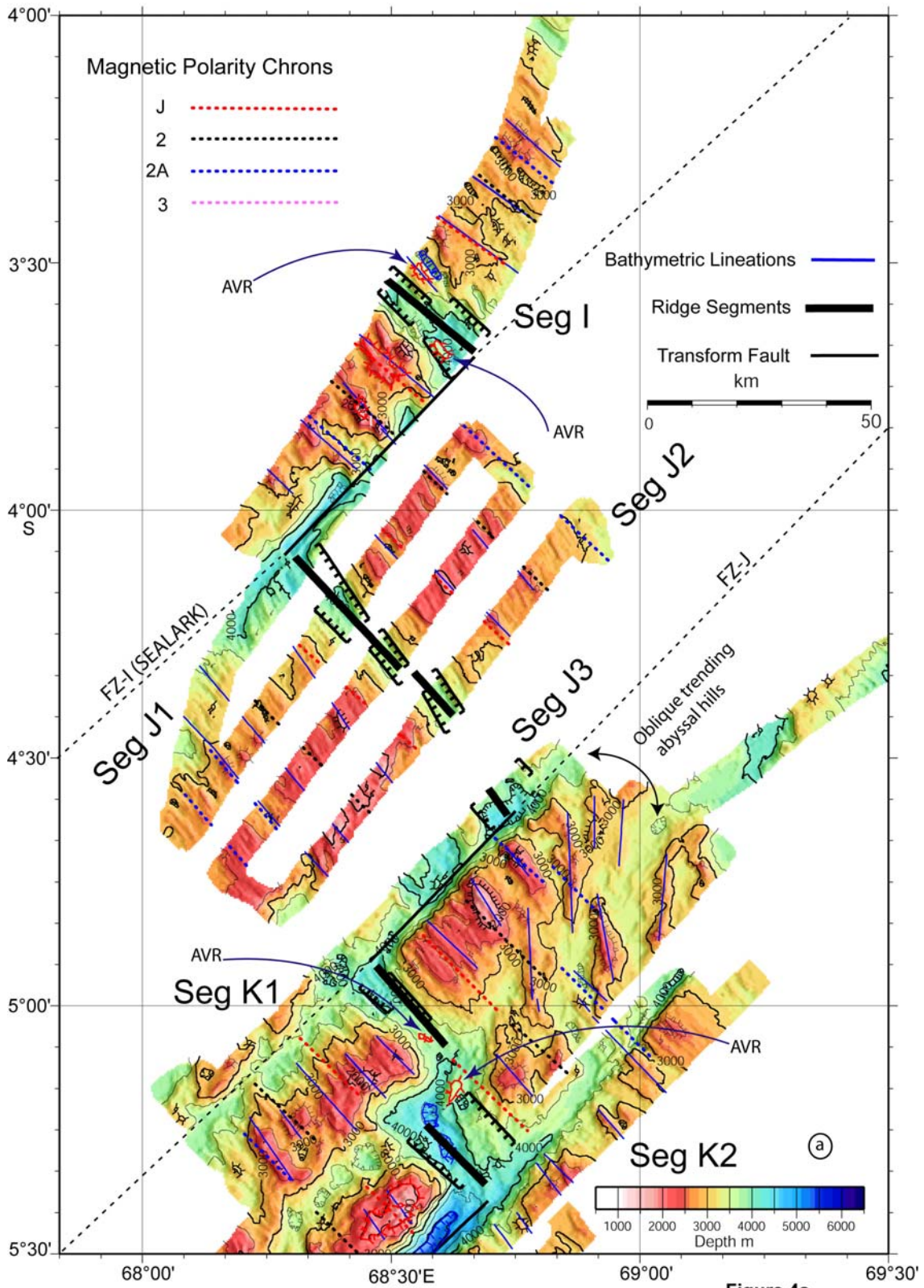
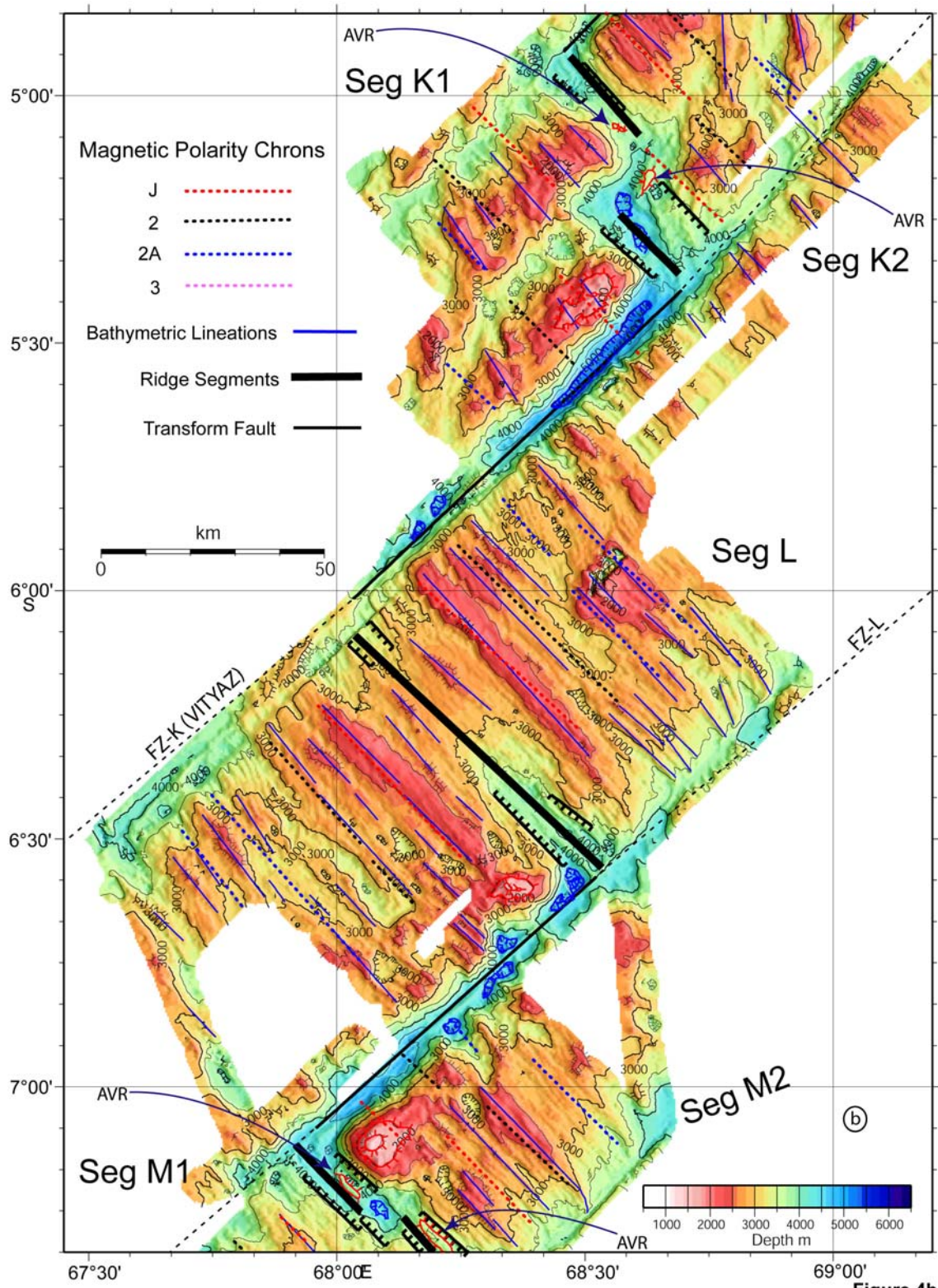


Figure 3





(b)

Figure 4b

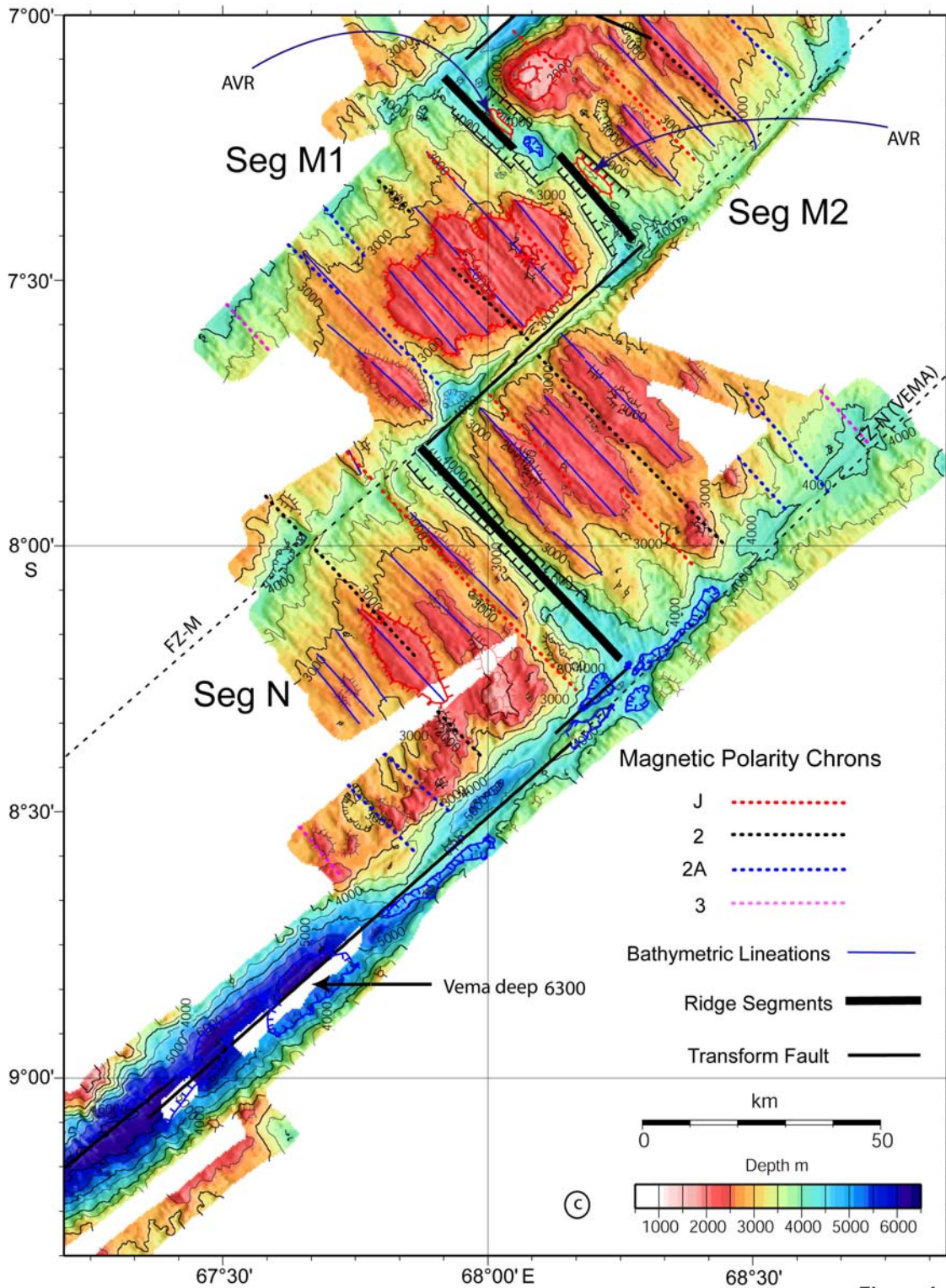


Figure 4c

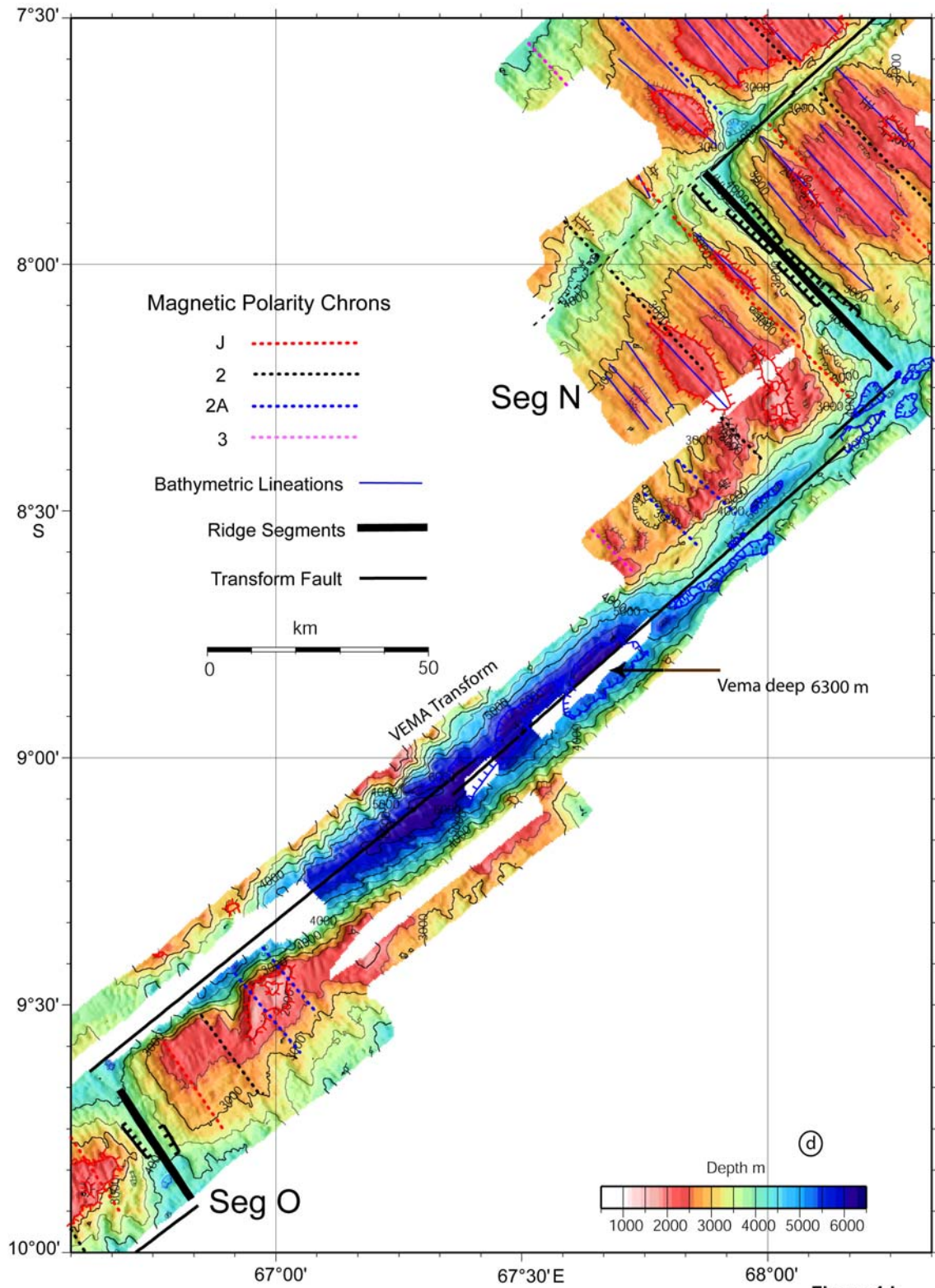
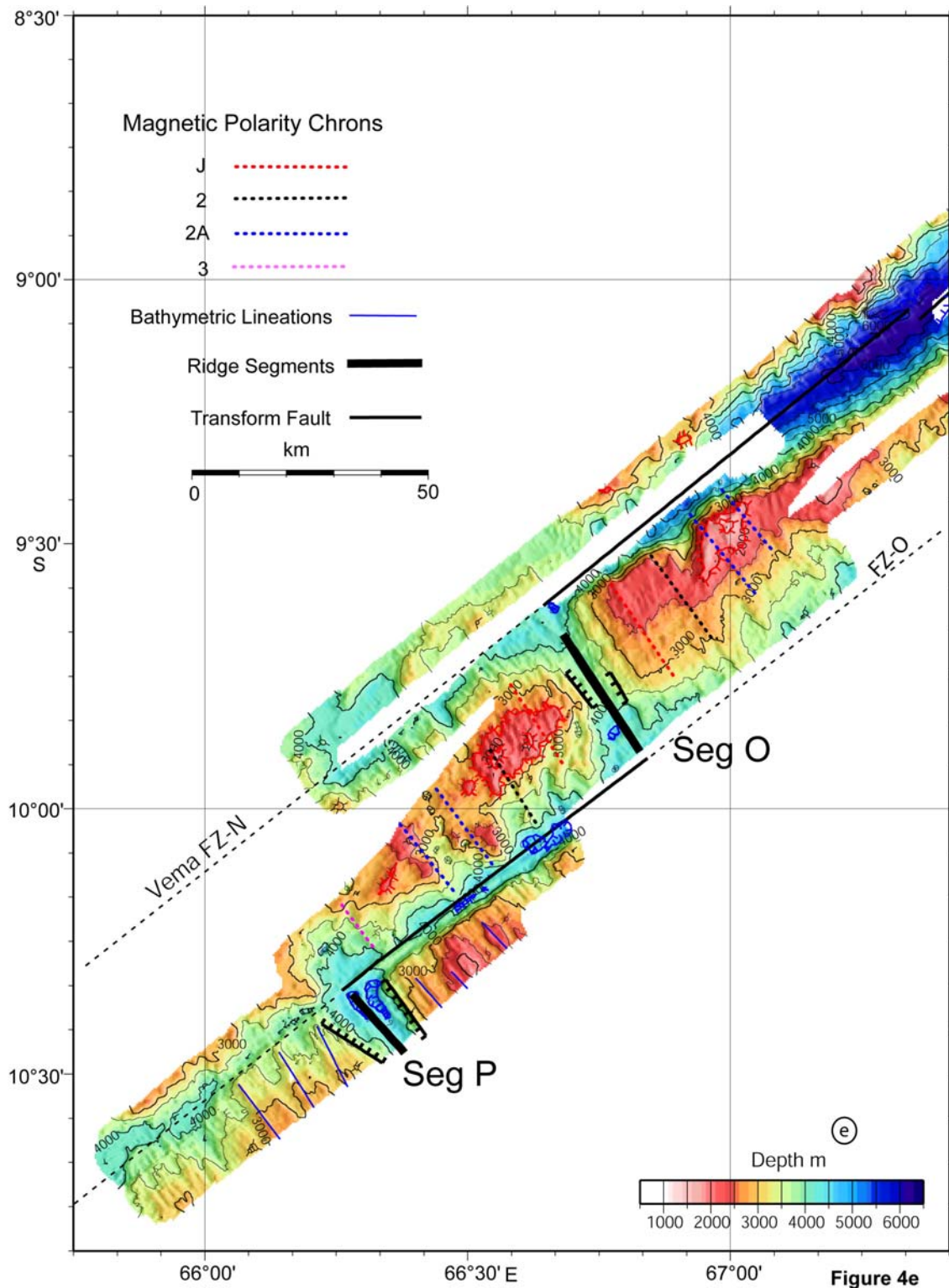


Figure 4d



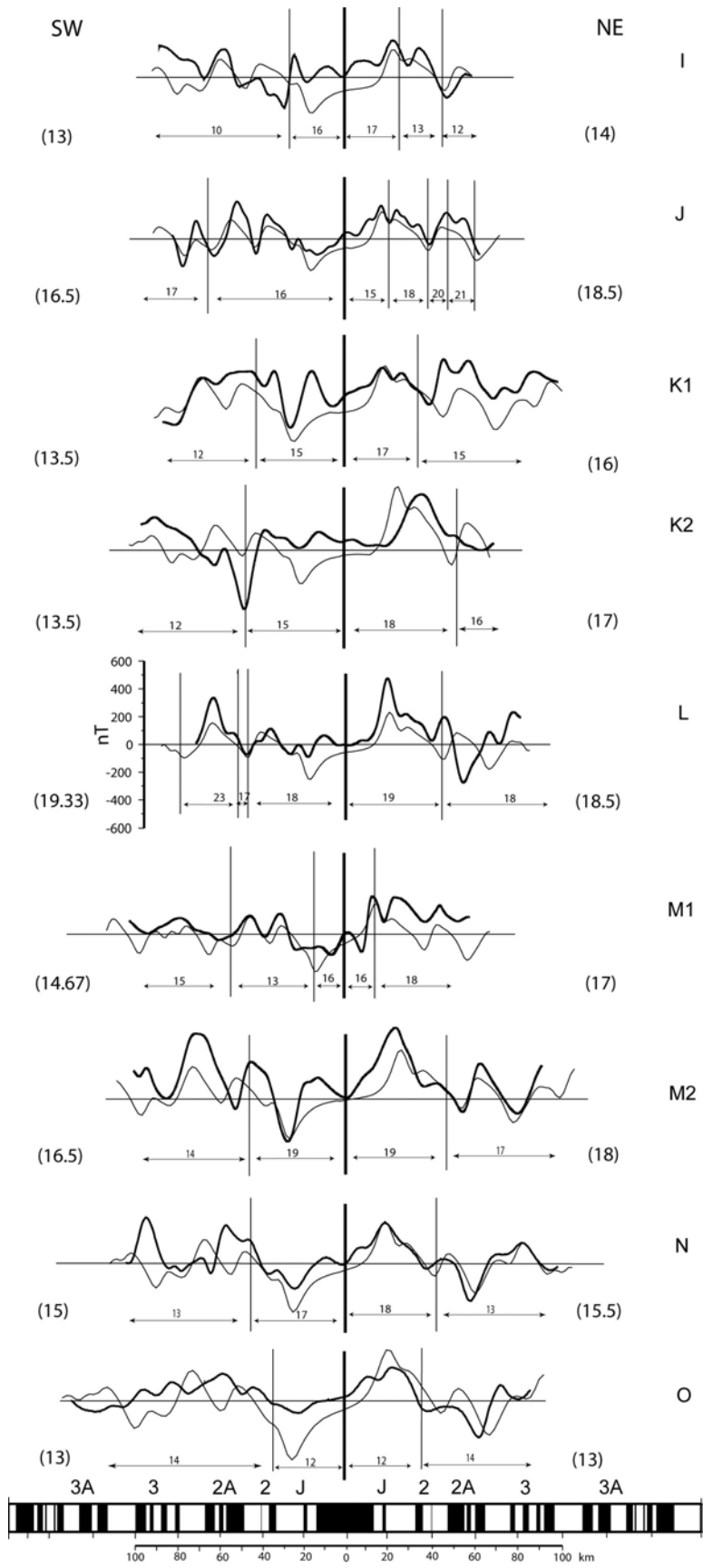


Figure 5

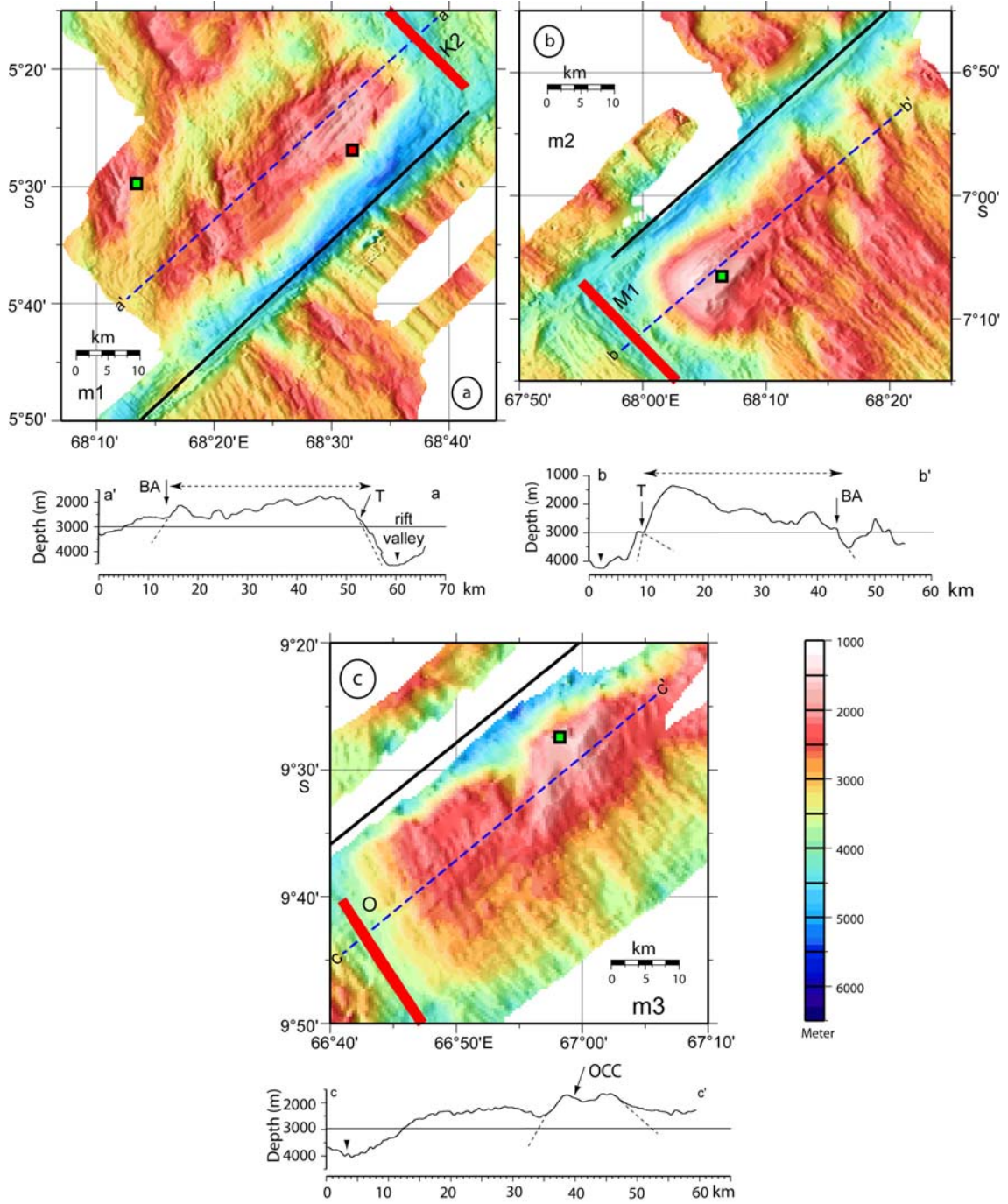


Figure 6